



Modeling of a novel SCHOTT B270 prism based SPR sensor using Ag-Si-BP/MXene structure for detection of specific biological samples

Yesudasu Vasimalla¹ · Himansu Shekhar Pradhan²

Received: 31 December 2021 / Accepted: 13 July 2022 / Published online: 19 August 2022

© The Author(s), under exclusive licence to Springer Science+Business Media, LLC, part of Springer Nature 2022

Abstract

This paper bestows a numerical modeling of novel SCHOTT B270 prism-based surface plasmon resonance (SPR) sensor to detect the specific biological samples, such as hemoglobin (HB) in blood and urine glucose level. The proposed structure is portrayed based on Kretschmann configuration and is comprised of the prism, silver (Ag), silicon (Si), black phosphorus (BP)/carbides and nitrides (MXene) and sensing medium. In this juncture, two different structures, such as structure-I and II, have been made by deploying the above-defined layers. The transfer matrix theory and the angular interrogation technique are exploited to investigate the SPR performance at 633 nm wavelength. The performances of the B270 and familiar BK prism-based structures are compared and endorsed the B270 prism-based structure yields better performance. Moreover, the SPR performance parameters for detection processes of HB in blood and urine glucose level have been computed for a range of refractive indices of their concentration levels. Results reveal that the maximum sensitivity (S) of 315.79 deg/RIU, dip-of-figure-of-merit (DFOM) of 38,583,333.33, quality-factor (QF) of 46.10 RIU⁻¹, and detection-accuracy (DA) of 0.837 for the HB detection process. Similarly, the maximum S of 310 deg/RIU, DFOM of 1,350,000.00, QF of 43.18 RIU⁻¹, and DA of 0.518 for the detection process of urine glucose level. Finally, the comparative study has been carried out at the end. Therefore, the proposed study provides the high-performance carrier for the detection of HB in blood and urine glucose level, and made a new way for the field of biomedical and biological.

Keywords SCHOTT B270 prism · Hemoglobin · Urine glucose · Sensitivity · Surface plasmon resonance · Transfer matrix theory

This article is part of the Topical Collection on Photonics: Current Challenges and Emerging Applications.

Guest edited by Jelena Radovanovic, Dragan Indjin, Maja Nesic, Nikola Vukovic and Milena Milosevic.

✉ Yesudasu Vasimalla
vasimalladasu@gmail.com

Extended author information available on the last page of the article

1 Introduction

Nowadays, the surface plasmon resonance (SPR) sensor is emerged as a highly promising sensing device in real-time due to its label-free detection, reliability, small sample size and accurate outcomes (Mitu et al. 2022). Generally, it executes to monitor the biomolecular interactions like specific biological samples (like urine glucose, hemoglobin (HB) in blood) (Sharma and Pandey 2018; Ahmed et al. 2019a; Jabin et al. 2019a). It also has a variety of gas sensing applications (Paul et al. 2018), and biomedical (Jabin et al. 2019b) and biological uses, including as medical diagnostics (Ahmed et al. 2019b), food safety (Ahmed et al. 2019c) and environmental monitoring (Lee et al. 2011). The SPR is a refractive index-based sensor that can detect minor changes in the refractive index of a given structure (Ahmed et al. 2021). In reality, the SPR parameters are determined by observing changes in the structure that correlate to changes in the refractive index (RI). The SPR sensor may be classified into four categories based on how it couples light: prism-based, fibre optic-based, waveguide-based and grating-based (Mitu et al. 2021). Literature reported that the prism-coupled SPR sensor achieves a greater sensitivity performance than other devices because of its high efficient light coupling (Jabbari et al. 2016). The SPR-based sensor has been introduced in the form of two configurations, (i) Kretschmann configuration and (ii) Otto configuration (Kretschmann and Raether 1968; Otto 1968). Since it has been a high efficient coupling at the P-M interface, the Kretschmann is preferable design structure rather than the Otto configuration (Homola 2006).

Furthermore, the surface plasmons (SPs), which are used to operating the SPR sensor, are excited by the oscillations of quanta-free electrons on the "prism-metal interface". These quanta electrons that are in the "conduction band" of the SPR active metal should be able to resonant with a certain angle of incoming light to activate the SPs. Due to its oscillations normal to the surface, the surface plasmon wave (SPW) is generated at the metal and dielectric interface, and the SPW yields the evanescent wave, which is declined exponentially (Homola 2004). The SPR mechanism is relying on the phase matching condition, where the propagation constant (PC) of the evanescent wave horizontal component (k_{ev}) is equal to the PC of SPW vector (k_{sp}), (i.e., $k_{ev} = k_0 \sqrt{\epsilon_p} \sin \theta_{res} = k_{sp}$). Where, $k_0 = \omega/c$ is the incident wave vector, ω is the angular frequency, c is the light speed, ϵ_p is the prism permittivity, and θ_{res} is resonance angle. At this state, the maximum incident light energy absorbs by the SPW, resulting in a decrease in the reflected wave intensity that is well-known as the minimum reflectance (R_{min}). The angle at where the R_{min} is obtained can be defined as the "resonance angle (θ_{res})" (Massson 2017). Many other researchers reported the SPR sensor furnishes the accurate outcomes with the angular interrogation method, whereas the SPR curve is a familiar relationship between reflectance intensity and angle (Vasimalla et al. 2021a). The discovered resonance dip angle varies with respect to the RI changes in the SPR structure, and the amount of change in resonance dip measures by using the sampling technique of "attenuated total internal reflectance (ATR)" (Said et al. 2015).

Usually, the gold (Au) deposits as metal film over the prism surface to excite the SPs (Zakaria et al. 2022). In (Yola et al. 2014), an Au-based sensor is proposed and determined "Amikacin (AMIK)" successfully in a human plasma sample. Similarly, another Au-based biosensor is presented using graphene and provided an excellent SPR performance for breast cancer detection (Hossain et al. 2019a). The authors in Biednov et al. (2015) made an enhanced Au metal film-sensing surface, which owns a high biomolecular absorption capability. However, Au has several disadvantages, such as a wider SPR curve, which might reduce resolution performance. To increase the resolution performance, a different

metal film, silver (Ag), can be used instead of Au since it has a higher SPR ratio and so gives greater plasmonic effect and narrowness than Au (Jabin et al. 2022). Moreover, the use of different metal oxides or high RI silicon (Si) over the metal layer can also greatly improve the sensitivity (S) of the biosensor (Cai et al. 2021). The absorption capacity of the sensor can be increased further by adding "two-dimensional (2D) materials (like graphene and molybdenum disulfide (MoS_2), black phosphorus (BP) and carbides and nitrides (MXene))". These materials are acted as "biomolecule recognition element (BRE)" as well as a protection layer (Farimani et al. 2014). Large-scale binding and adsorbent material are two crucial components for SPR-related sensors. For a while, graphene and MoS_2 are usually adopted as a 2D-nano-material, and have a high carrier mobility as well as optical transparency. Also, they are extensively active in optoelectronic applications, such as photodetectors, touch screens, polarizers and optical modulators (Mishra et al. 2016). Nowadays, due to various different mechanical and optoelectrical features, such as large bandgap, black phosphorus (BP) has become a most desirable 2D nano-material in photonic sensors. Added to that, BP increases the sensing capacities by amplifying interlayer coupling within the van der Waals forces. Because of the BP has a larger adsorption energy than graphene and MoS_2 , it is excellent for biomolecule binding (Cho et al. 2016). In (Mao et al. 2016; Wu et al. 2017), the SPR sensors are presented employing the heterostructure of "few-layer BP-graphene/TMDC materials", and found the enhanced S. In the realm of biosensing, the combination of Ag-BP structure is the most robust and effective (Liang et al. 2020). Recently, an Ag-BP based SPR biosensor is fabricated (Cho et al. 2016), and examined its performance in terms of S of $130^\circ/\text{RIU}$ and "figure of merit (FOM)" of 61 using six layers of BP (Rahman et al. 2019).

Moreover, a new member in the family of 2D nanomaterials, MXene- $\text{Ti}_3\text{C}_2\text{Tx}$, has been recently earned significant interest due to its layered nature, hydrophobicity, exceptional mechanical strength, attractive electrical and plasmonic properties. The properties of MXene are influenced by its surface terminations, which can have a significant impact on its plasmonic capabilities. Consequently, their surface termination affects the SPR sensor (Xin et al. 2020). A. Srivastava et al. proposed an Au-based SPR sensor employing MXene and BP and achieved a better S of $190.22 \text{ deg}/\text{RIU}$ (Srivastava et al. 2020). Also, M. K. Singh et al. suggested a highly performed bi-metal layer-based SPR sensor using BP and MXene, and results found the highest S of $304 \text{ deg}/\text{RIU}$ (Singh et al. 2021). Moreover, Kumar et al. explored another SPR sensor based on the hybrid nanostructure of BP and MXene and achieved the maximum S of $264 \text{ deg}/\text{RIU}$, whereas BP layers play a crucial role in it (Kumar et al. 2021). Since detection of specific biological samples plays a key role in the biomedical field, recently, S. Mustafa et al. proposed the graphene-coated SPR sensor to detect specific biological samples (Shahriar et al. 2021). However, succession is still a prerequisite for the researchers in order to improve the performance characteristics as well as the sensors' progress.

Therefore, we presents a novel SCHOTT boron 270 (B270) prism-based SPR sensor to improve the performance and shows sensor's progress. The B270 prism has the strong technical credentials, including remarkable optical performance in a broad range thicknesses and suitable for wider range applications due to its highly transparent, super-white soda-lime glass and high quality at an inexpensive cost. In this paper, a high sensitive and standard sensing accuracy along with the good quality novel B270 prism-based SPR sensor is proposed employing Ag-Si-BP/MXene structure to detect specific biological samples. This is the first time the multi-purpose glass of SCHOTT B270 prism is employed in the SPR sensor for the biological interactions. The paper has been arranged as follows: Section-2 deals with the study of the specific biological samples; section-3 explains the design

and methodology; section-4 exhibits the results and discussion; and finally, section-5 concludes the proposed work.

1.1 The fabrication process

To prepare the sensor, Ag metal layer can be deposited on a prism surface by using the physical “vapor deposition technique (VDT)”. The Silicon (Si) layer will be deposited on top of the metal layer. Before dip coated, the coated Ag is engrossed in the Si suspension for 20–30 s. Then, the Si will be annealed at 50 °C for 2–3 h before it being used. The multilayered BP/MXene can be equipped by etching through a minimally intensive layer delamination (MILD) procedure. Let’s consider for the MXene preparation. Firstly, “2gm of LiF was added to 40 mL of HCl (6 mol/L). After stirring at room temperature for 5 min, 2 g of Ti_3AlC_2 was added, and the mixture was continually stirred at 35 °C for another 24 h. The flask cover was kept tight during the reaction to prevent the volatilization of HCl. After etching, the mixture was washed repeatedly by water (350 mL, 350 mL) until the pH value reached 6. The mixture was then centrifuged for one hour at 3500 rpm to obtain a multilayered MXene supernant, which was further dip-coated onto the surface of a highly reflecting gold mirror for further characterizations and applications. The MXene can be prepared by extracting Al from the corresponding MAX phase (Ti_3C_2Tx) using hydrofluoric (HF) acid, and then monolayer Ti_3C_2Tx can be obtained by employing the liquid phase exfoliation method. The Ti_3C_2Tx can be deposited on Ga-doped substrates using an optical deposition technique” (Kumar et al. 2022). Further, the synthesized MXene is placed on the top of Si along with the metal deposited prism surface. Finally, a sensor chip is placed on the rotaray stage of the experiment setup for the detection of HB in blood and urine glucose level, as done by authors in Maurya and Prajapati (2020).

2 Study of specific biological samples

The evaluation study of the specific biological samples, such as the hemoglobin (HB) in blood and urine glucose levels, is explained in this section.

2.1 Blood hemoglobin level

Blood is an essential component in human beings and it is the exclusive body fluid for judging a human body’s physiological condition. Hemoglobin (HB) is the protein molecule that originated in the red blood cell (RBC). It transfers the oxygen from the lungs to the human tissues and reflects the carbon dioxide in vice versa. To achieve optimal oxygenation of the tissue, a sufficient amount of HB should be maintained. HB levels in the blood are usually measured in grams per liter (g/l). The average range of HB level for males is 140 to 180 g/l, whereas it is 120 to 160 g/l for females. The low level of HB indicates the patient is diagnosed with anemia, while the high HB level means the polycythemia that causes the body to make too many red blood cells. The changes in HB level lead to several diseases like heart attacks and strokes (Perez et al. 2013). Therefore, it is necessary to detect the blood HB level for controlling the human body physiological conditions. According to the reference (Sani and Khosroabadi 2020a), an average person’s blood refractive index (RI) ranges from 1.32919 to 1.34995, and every 0.001 RI change in the blood causes a 6.1025 g/l increase in HB. Figure 1 shows the relationship between the HB

concentration and its RIs, observing the linear relationship. This relation can be obtained from $B_r = B_0 + C\Delta n$, whereas B_r is the resultant blood HB level, B_0 is the present blood HB level, C is the constant value of 5766.5 and Δn is the RI change. To compute the blood HB level, the RBC preprocessing of blood samples is essential because that the direct process of detecting blood HB samples can offers an error in the measurement (Perez et al. 2013; Sani and Khosroabadi 2020a). Ajad et al. has recently proposed a whispering gallery mode based sensor to detect the blood HB level and found that low performance for only a RI variation of 0.0044 (Ajad et al. 2021).

2.2 Study of glucose level in the urine

The high blood glucose (blood sugar) levels are indicating diabetes, which is a chronic metabolic disease that releases several severe problems with the heart, eyes, blood, kidneys and brain system (Jouven et al. 2005). According to the world health organization (WHO), around 422 million people worldwide have diabetes, and it is directly responsible for 1.6 million deaths each year (Sani and Khosroabadi 2020b). The RI of the body fluids, including urine, varies from each human being due to changes in the glucose concentration levels. Hypoglycemia is defined as a blood glucose level of less than 0.04 gm/dl (gram/deciliter), whereas hyperglycemia is defined as a blood glucose level of more than 0.279 gm/dl (Sani and Khosroabadi 2020a). Generally, a human body contains a glucose level of more than 0 to 0.015 gm/dl, but it increases due to glycosuria in urine with an average range of 0.165 to 0.180 gm/dl. Figure 2 depicts the relationship between the glucose concentration level and its RI, which is obtained from Jouven et al. (2005). Sani et al. have explored a recent study on the detection of glucose concentration using photonic crystal fiber Nano-cavity, whereas it is more costly and complex (Sani and Khosroabadi 2020b).

3 Design and methodology

In this section, we discuss the design considerations and mathematical modeling for computing the reflectivity as well as sensing parameter of the proposed SPR sensor.

Fig. 1 HB concentration increment versus Refractive index relation

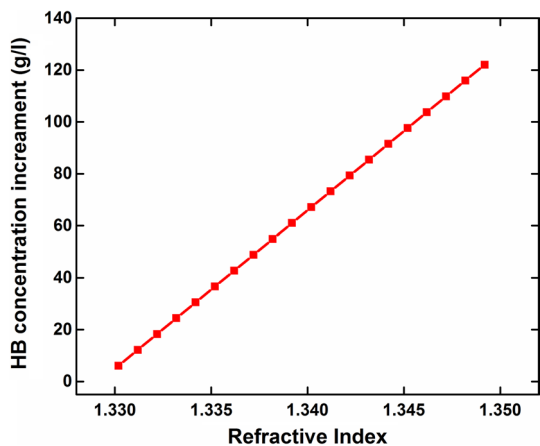
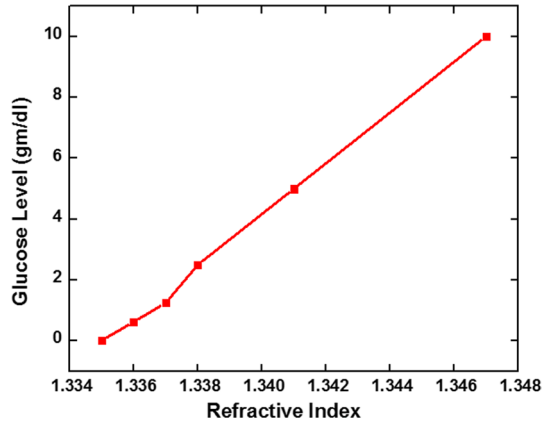


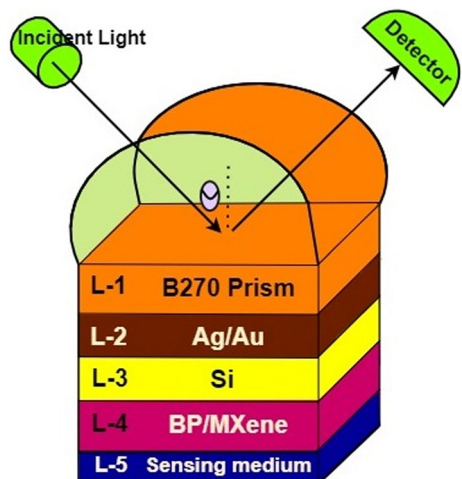
Fig. 2 Glucose level in urine versus Refractive index relation



3.1 Design considerations

The schematic proposed SPR structure is depicted in Fig. 3 to detect the blood HB level and urine glucose level. The ultra-white crown glass (SCHOTT B270) is used as the coupling prism (first layer) for the proposed structure, having the RI of 1.523 at 633 nm wavelength (λ), where it can furnish minimum Kerr effect (Vasimalla et al. 2021b). To compare the optimal performance of the proposed prism-based structure, we have considered the familiar prism-based structure in SPR, i.e., of BK7, having the RI of 1.515 (Rahman et al. 2019). As the second layer, the metal film of Ag is coated on the prism surface for higher surface plasmon polaritons (SPPs) excitation with the RI of $0.056206 + 4.2776i$ (Otto 1968; Wu et al. 2017). The RIs for Ag can be obtained from the Drude–Lorentz model, showing in Eq. (1). Where λ_c and λ_p represent the collision and plasma wavelengths, and their values are 1.7614×10^{-5} m and 1.4541×10^{-5} m, respectively (Vasimalla et al. 2021b). To prevent the susceptibility to oxidization and sharper resonance dip, the proposed structure is covered the metal film surface with Si, having the RI of 3.916 at the defined-wavelength (Klantsataya et al. 2015). The thicknesses of metal film and Si are optimized for each structure that show in further analysis of

Fig. 3 The schematic structure proposed SPR sensor for detection of blood hemoglobin level and urine glucose level



the proposed sensor. According to the literature, the best SPR performance is attained when the metal film thickness is between 40 and 50 nm, whereas Si thickness varies depending on the top-coated layers. Furthermore, as fourth layer, the 2D TMDC material of BP or MXene is utilized for enhancing the biomolecule adsorption, and having the refractive indexes of $3.0 + 1.149i$ and $2.38 + 1.33i$, and thickness of 0.53 nm and 0.993 nm for BP and MXene, respectively (Wu et al. 2017; Liang et al. 2020). Finally, as the fifth layer, the sensing region is occupied with biomolecules samples, such as HB in blood and urine glucose. The RI of the sensing region is given as $n_{sensing} = n_0 + \delta n$, where $n_{sensing}$ is the sensing RI, n_0 is reference RI and δn is the change in the RI from the reference RI (Farimani et al. 2014; Sani and Khosroabadi 2020a).

$$n_{AG} = \left(1 - \frac{\lambda^2 \lambda_c}{\lambda_p^2 (\lambda_c + i\lambda)} \right)^{1/2} \tag{1}$$

3.2 Methodology

The R_{min} of SPR reflectance curve transpires at the resonance condition, where the propagation constant (PC) of k_x is equal to PC of the wave vector of SPs (k_{SPW}) that governs by the theta. Its mathematical expressions are mentioned in Eqs. (2) and (3) (Rahman et al. 2017a). Where, n_{Ag} , n_{Si} and n_s are the RIs of the Ag, Si and sensing medium, respectively.

$$k_x = k_{SPW} \frac{2\pi}{\lambda_{633}} \tag{2}$$

$$(n_p \sin \theta) = \frac{2\pi}{\lambda_{633}} \sqrt{\frac{n_{Ag}^2 n_{Si}^2}{n_{Ag}^2 + n_{Si}^2}} \tag{3}$$

The θ_{SPR} is an angle where the R_{min} is achieved and it can be evaluate by using Eq. (4) (Rahman et al. 2017a; Hossain et al. 2019b).

$$\theta_{SPR} = \left(\sin \sqrt{\frac{n_{Ag}^2 n_s^2}{n_{BK7}^2 (n_{Ag}^2 + n_s^2)}} \right)^{-1} \tag{4}$$

To evaluate the sensor’s reflectivity in terms of an angle, this study has considered the Fresnel model analysis of multilayer reflection theory and the transfer matrix method (TMM). The relation between the reflectance intensity (R_p) and the incidence angle is well-known the SPR curve. The mathematical expressions for computing the R_p and reflection coefficient (r_p) are shown in Eqs. (5) and (6), respectively (Hossain et al. 2019b).

$$R_p = r_p r_p^* = |r_p|^2 \tag{5}$$

$$r_p = \frac{(H_{11} + H_{12}n_N) - (H_{21} + H_{22}n_N)}{(H_{11} + H_{12}n_N) + (H_{21} + H_{22}n_N)} \tag{6}$$

Equation (7) signifies a description of the transverse RI (n_k) for the corresponding k^{th} layer (Hossain et al. 2019b).

$$n_k = \left[\frac{\mu_k}{\epsilon_k} \right]^{1/2} \cos \theta_k = \sqrt{\frac{\epsilon_k - (n_p \sin \theta)^2}{\epsilon_k^2}} \tag{7}$$

H_{if} shows the properties matrix of the SPR sensor combined structure, and for P-polarized incident light, it can be destined by Eq. (8) (Farimani et al. 2014; Kumar et al. 2021).

$$H_{if} = \left[\prod_{k=2}^{N-1} \begin{pmatrix} \cos \beta_k - i \sin \beta_k & \\ -in_k \sin \beta_k \cos \beta_k & \end{pmatrix} \right]_{if} = \begin{bmatrix} H_{11} & H_{12} \\ H_{21} & H_{22} \end{bmatrix} \tag{8}$$

where β_k is the arbitrary stage constant for k^{th} layer and numerically expressive in Eq. (9) (Rahman et al. 2017b):

$$\beta_k = \frac{2\pi}{\lambda} n_k \cos \theta_k (z_k - z_{k-1}) = \frac{2\pi}{\lambda} d_k \sqrt{\epsilon_k - (n_p \sin \theta)^2} \tag{9}$$

And, z_k is the wave impedance of k^{th} layer and mathematically represented in Eq. (10) (Rahman et al. 2017b).

$$z_k = \frac{k_x n_k \cos \theta_k}{(2\pi c / \lambda_{633}) \epsilon_k^2} \tag{10}$$

Finally, in the Eq. (12) the input angle of θ_k for a k^{th} layer can be shown as follows (Rahman et al. 2017b).

$$\theta_k = \left(\cos \sqrt{1 - (n_{k-1}/n_k)(\sin \theta)^2} \right)^{-1} \tag{11}$$

where ϵ_k , μ_k and d_k are the permittivity, permeability and thickness of k^{th} layer.

After substituting all defined parameters in Eq. (5), the mathematical expression for computing reflectivity of the proposed sensor, which has five layers structures, is shown below Eq. (12) (Vasimalla et al. 2021b).

$$R_{12345} = |r_{12345}|^2 = \left| \frac{r_{12} + r_{2345} e^{2ik_2 d_2}}{1 + r_{12} r_{2345} e^{2ik_2 d_2}} \right|^2 \tag{12}$$

$$r_{2345} = \frac{r_{23} + r_{34567} e^{2ik_3 d_3}}{1 + r_{23} r_{34567} e^{2ik_3 d_3}}, r_{345} = \frac{r_{34} + r_{45} e^{2ik_4 d_4}}{1 + r_{34} r_{45} e^{2ik_4 d_4}}, r_{12} = \frac{\epsilon_2/K_2 - \epsilon_1/K_1}{\epsilon_2/K_2 + \epsilon_1/K_1},$$

$$r_{23} = \frac{\epsilon_3/K_3 - \epsilon_2/K_2}{\epsilon_3/K_3 + \epsilon_2/K_2}, r_{34} = \frac{\epsilon_4/K_4 - \epsilon_3/K_3}{\epsilon_4/K_4 + \epsilon_3/K_3}, r_{45} = \frac{\epsilon_5/K_5 - \epsilon_4/K_4}{\epsilon_5/K_5 + \epsilon_4/K_4}$$

r_{12}, r_{23}, r_{34} , and r_{45} are the reflected amplitudes from 1–2, 2–3, 3–4, 4–5 layers, respectively. Where d_m denotes thickness of each layer ($m = 2, 3, 4, 5$).

3.2.1 Performance parameters of the proposed SPR sensor

The S is a crucial factor for a better SPR sensor, and is defined as the ratio of change in SPR resonance angle ($\nabla\theta_{res}$) to change in the RI (∇n). Higher S performance of a sensor with a little change in analyte (biomolecules) concentration indicates that the sensor has superior detecting capabilities since it can detect extremely minute structural variations. Furthermore, the results of this study compute the “dip of figure of merit (DFOM)”, “quality factor (QF)”, and “detection accuracy (DA)”, exhibiting the product quality, noise influence, and sensor accuracy. The mathematical expressions to compute the above-defined parameters are shown in Eq. (13–16), whereas FWHM is the full width half maximum (Vasimalla et al. 2021b, 2020).

$$\text{Sensitivity (S)} = \frac{\text{Change in resonance angle } (\nabla\theta_{res})}{\text{Change in refractive index } (\nabla n)} \text{ (deg/RIU)} \quad (13)$$

$$\text{Dip of Figure of Merit (DFOM)} = \frac{S}{\text{Minimum Reflectance } (R_{min})} \quad (14)$$

$$\text{Quality Factor (QF)} = \frac{S}{\text{Full width half maximum (FWHM)}} \text{ (RIU}^{-1}\text{)} \quad (15)$$

$$\text{Detection Accuracy (DA)} = \frac{\nabla\theta_{res}}{\text{FWHM}} \quad (16)$$

4 Results and discussions

4.1 Optimization of layers thicknesses for SPR structure

Since the metal film’s nature varies according to the nature of top dielectric material (Sani and Khosroabadi 2020a), this section investigates the optimization of the Ag and Si layers thicknesses for optimal performance. The optimization is observed from the performance of R_{min} (should be as low as possible) (Vasimalla et al. 2021b; Mudgal et al. 2020) using the Fresnel model analysis of multilayer reflection theory. The less R_{min} shows the maximum light energy transfer to the SPW that leads to higher SPR performance. We have presented this work by proposing two structures, such as structure-I and structure-II, and respected configurations are mentioned in Table 1.

Table 1 Different structures numbers and name and configurations

Structure number and name	Configuration
I. Ag-Si-BP based SPR	Prism-Ag-Si-BP-Sensing
II. Ag-Si-MXene based SPR	Prism-Ag-Si-MXene-Sensing

Fig. 4 Reflectance versus angle for different metal film thicknesses to obtain optimized metal thickness **a** Ag **b** Au

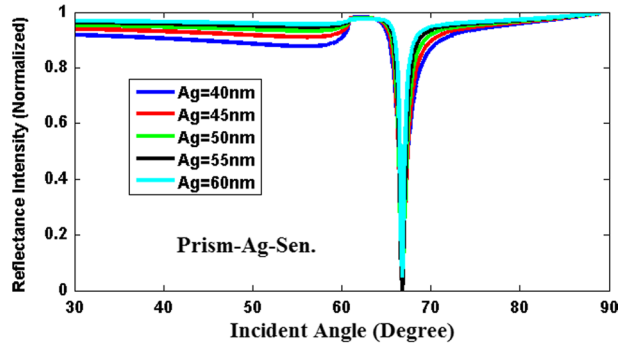
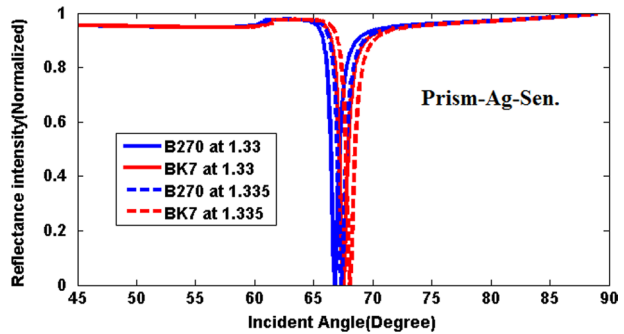


Fig. 5 Reflectance curves in terms of an angle for different conventional SPR structure using B270 and BK7 prisms at the sensing RIs of 1.33 and 1.335 (Prism-Ag-Sensing medium at Ag thickness of 55 nm)



4.1.1 Performance analysis of prism-based structures: Optimized Ag thickness

The conventional SPR structure is considered to optimize Ag thickness and coupling-prism. Figure 4 depicts the reflectance curves of the conventional SPR structure (B270 prism-Ag-sensing) are plotted at different Ag thicknesses (40 nm to 60 nm with interval of 5 nm). In the event, the asymmetrical property in the SPR curves can be observed, which occurs due to the changes in the layer thickness and the SPs' spatial extension in a medium. The least R_{\min} of 0.0030 is attained at the Ag thickness of 55 nm, as shown in Fig. 4, whereas it increases at the residual events. The less R_{\min} is transpired due to the low absorption loss and spatial extension of SPs that depends on its propagation length (PL) in the parallel direction (Maurya and Prajapati 2017 Aug). In summary, the optimized thickness of Ag is 55 nm for the conventional SPR sensor in order to excite the higher SPs.

Furthermore, to optimize the coupling-prism, Fig. 5 represents the reflectance curves in terms of an angle for two different prism based structures at the sensing RI of 1.33 and 1.335: (i) BK7-Ag-sensing structure (mostly utilized structure in the SPR field) and (ii) proposed B270-Ag-sensing. From Fig. 5, the obtained resonance angles are 66.79 and 67.33 deg at the sensing RI of 1.33 and 1.335, respectively. The S parameter is computed using Eq. (13) and found that the S of 108 deg/RIU for B270-Ag-sensing, and 106 deg/RIU for BK7-Ag-sensing structures. This performance witnesses that the B270-Ag-sensing based SPR sensor offers higher performance compared to the BK7-Ag-sensing based SPR sensor due to higher absorption molecules (Wu et al. 2017; Ajad et al. 2021). Therefore, the optimal structure of B270-Ag-sensing is utilized for further investigation of this study.

4.1.2 Optimization of Ag, Si thicknesses for Ag-Si-BP-based structure

The optimized structure is required for the detection process, therefore, the optimization of the Ag and Si thicknesses are performed in this section employing structure-I and II. Figure 6 represents the structure-I's reflectance curves for different Si layer thicknesses (Si: 1 to 8 nm with an interval of 1 nm) at different Ag thicknesses (Ag: 40 to 50 nm with an interval of 5 nm), where Fig. 6a for Ag of 40 nm, Fig. 6b for Ag of 45 nm and Fig. 6c for Ag of 50 nm. In this section, the thickness of BP layer is kept constant of 0.53 nm because it offers low absorption loss. The resonance dip and R_{\min} of SPR curves of Fig. 6 are asymmetrical due to the variations in the layers thicknesses that are make the corresponding changes in the SP's excitations, penetration depth and penetration length of the sensor. The obtained R_{\min} values for Fig. 6 are mentioned in Table 2 and noticed the less R_{\min} is furnished at the Ag and Si thicknesses of 45 nm and 6 nm, respectively. Therefore, these optimized thicknesses are utilized to analyze structure-I for specific biological samples detection.

4.1.3 Optimization of Ag, Si thicknesses for Ag-Si-MXene-based structure

Similarly, Fig. 7 shows reflectance curves in terms of an angle for the structure-II. In this event, the Ag and Si thicknesses are varied (Ag: 40–50 nm with an interval of 5 nm, and Si: 1–7 nm with an interval of 1 nm). The obtained R_{\min} values for Fig. 7 a-c are reported in Table 3 and it is found the less R_{\min} is fascinated at the Ag and Si thicknesses of 40 nm and 6 nm, respectively. Hence, these optimized thicknesses are employed to investigate structure-II for specific biological samples detection. In summary, the thicknesses of Ag, Si, BP and MXene for structure-I and II are reported in Table 4, which are used to execute the further analysis of the proposed sensor.

4.2 Performance analysis of blood HB level detection

The reflectance intensity curves for the considered two structures are exhibited in Fig. 8 at different HB level refractive indexes in order to detect it, where Fig. 8a for structure-I and Fig. 8b for structure-II. The samples of HB level are incorporated into the sensing surface, which is placed on the 2D material (BP/MXene) surface with an RI change of 0.001 (by cause of 6.1025 g/l increment in HB in blood). From Fig. 8, it can be observed the asymmetrical SPR dips and FWHM, which are due to the variations of the sensing RI and SP's excitation at the P-M interface (Wu et al. 2017). Moreover, the spatial extension of SPs in a medium causes a low R_{\min} , whereas a high R_{\min} and FWHM occur due to the attenuation or damping of electromagnetic wave effect (Klantsataya et al. 2015). From the obtained resonance angles and R_{\min} values of Fig. 8, the performances of S and DFOM are computed by using Eqs. (13) and (14), respectively, and these parameters are reported in Table 5.

The achieved sensitivities are varied in between 242 and 315.79 deg/RIU for structure-I, and 210.53 to 258.99 deg/RIU for structure-II in the detection process of HB in blood. Similarly, the obtained DFOMs are varied in between 2201.99 to 3,511,000.00 for structure-I, and 4658.09 to 38,583,333.33 for structure-II. The accomplished sensitivities and DFOMs are varied in both structures due to the absorption nature, RI and damping property of the 2D materials of BP and MXene (Ajad et al. 2021; Jouven et al. 2005). Moreover, the graphical representation of the S and DFOM variations for both structures

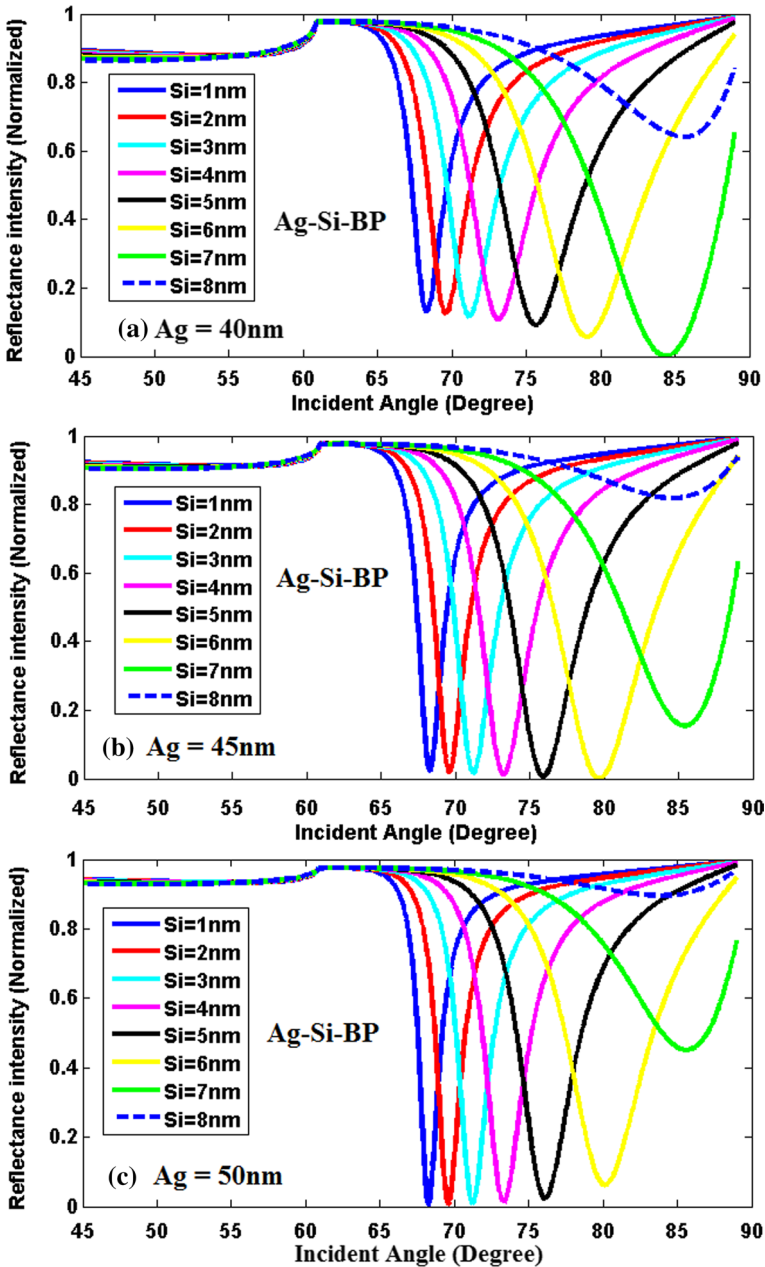


Fig. 6 Ag-Si-BP based structure’s reflectance curves using angular interrogation for different Si layer thicknesses at different Ag thicknesses **a** Ag of 40 nm **b** Ag of 45 nm **c** Ag of 50 nm

are represented in Fig. 9a; in addition, the performances of DA and QF are measured by using Eqs. (15) and (16), respectively, for both structures, as represented in Fig. 9b; the maximum achieved QF and DA are 46.10 RIU^{-1} and 0.837 for structure-I, 28.62 RIU^{-1}

Table 2 Measurement of R_{\min} values for different Ag and Si thicknesses of structure-I

Ag Thickness	R_{\min} values for respective Si thicknesses							
	1 nm	2 nm	3 nm	4 nm	5 nm	6 nm	7 nm	8 nm
Ag = 40 nm	0.1303	0.1248	0.1180	0.1082	0.0913	0.0569	0.0001	0.6407
Ag = 45 nm	0.0231	0.0202	0.0171	0.0124	0.0060	0.00007	0.1537	0.8181
Ag = 50 nm	0.0054	0.0067	0.0090	0.0134	0.0235	0.0621	0.4506	0.8955

and 0.549 for structure-II. From the observation of Table 5 and Fig. 9, it can be confirmed that the better performances of S, QF and DA can be achieved by employing structure-I, whereas better DFOM can be achieved by employing structure-II for detecting the HB in blood.

4.3 Performance analysis of glucose level in urine detection

To analyze the detect process of glucose level in urine, the reflectance intensity curves are plotted for two considered structures, as shown in Fig. 10, at different RI of the glucose concentrations, where Fig. 10a for structure-I and Fig. 10b for structure-II. Due to the SP's excitation at the P-M interface and sensing RI changes, Fig. 10 exhibits the nonsymmetrical SPR resonance dips, FWHM and R_{\min} . The obtained resonance angles and R_{\min} values are noted in Table 6, which is also noted the corresponding S and DFOM performances that are measured by applying Eqs. (13) and (14), respectively. In the glucose level in urine detection process, the accomplished sensitivities are 230 to 310 deg/RIU for structure-I, 250 to 270 deg/RIU for structure-II. Similarly, the obtained DFOMs are 3822.44 to 57,500.00 for structure-I and 8230.98 to 1,350,000.00 for structure-II. In addition, the performances of QF and DA are calculated by using Eqs. (15) and (16), respectively, and it is found the maximum achieved QF and DA performances are 43.13 RIU⁻¹ and 0.518, respectively, for structure-I, 29.13 RIU⁻¹ and 0.347, respectively, for structure-II. The graphical representations of S and DFOM, QF and DA with respect the glucose level RIs are shown in Fig. 11a, b. After observing the performance analysis, it can be witnessed that the better performances of S, QF and DA can be furnished by employing structure-I, whereas better DFOM can be furnished by employing structure-II for detecting the glucose level in urine.

4.4 Comparative study on performance analysis

The comparative study of the proposed sensor performance with existed work done by other researchers has been carried out in this section, as tabulated in Table 7. This study is witnessed that the proposed work with structure-I and II facilitates the better performances of S and DA compared to existed work. In HB in blood detection process, the better performances are S of 315.79 and DA of 0.837 for B270-Ag-Si-BP-Sensing (structure-I), S of 258.99 and DA of 0.549 for B270-Ag-Si-MXene-Sensing (structure-II). Similarly, in glucose level in urine detection process, the better performances are S of 310.00 deg/RIU and DA of 0.518 for structure-I, S of 270.00 deg/RIU and DA of 0.374 for structure-II. Moreover, this study is witnessed the proposed work is introduced the performances of QF and DFOM in the detection processes of specific biological samples for the first time compared

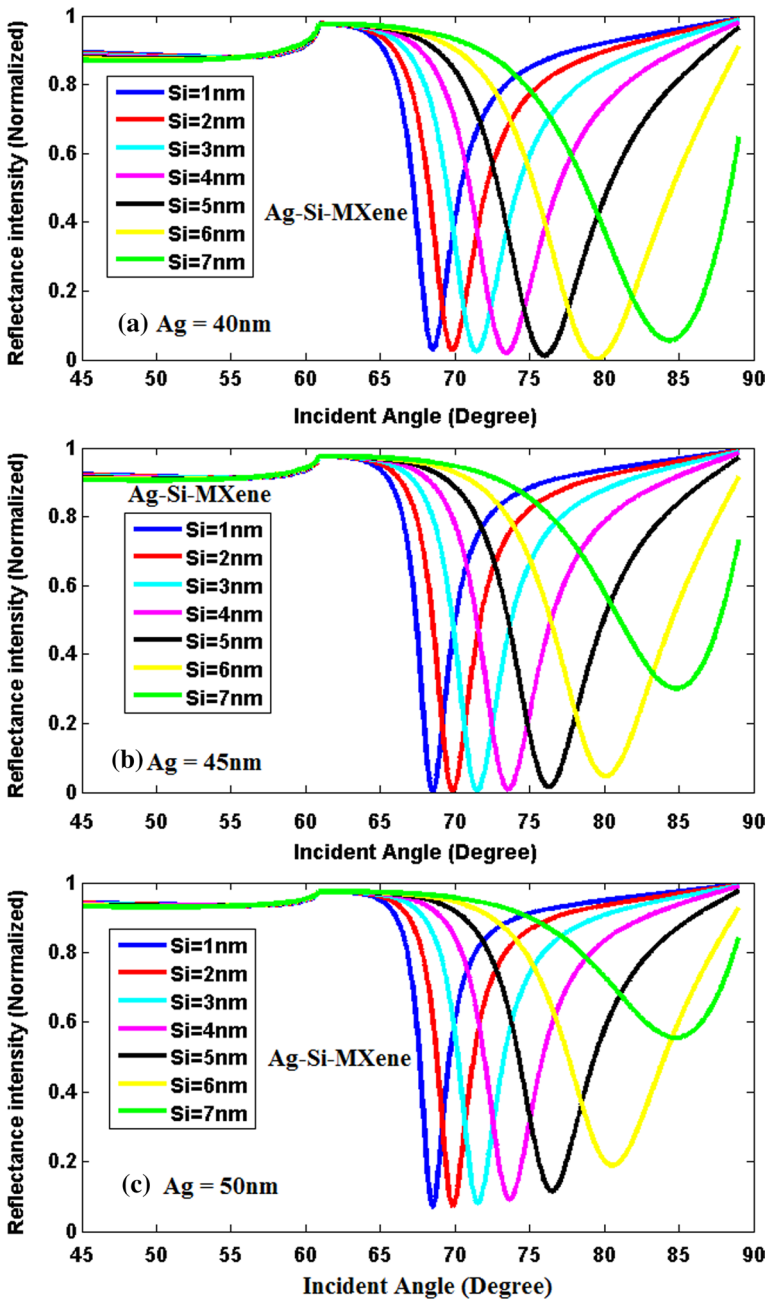


Fig. 7 Ag-Si-MXene based structure's reflectance curves using angular interrogation for different Si layer thicknesses at different Ag thicknesses **a** Ag of 40 nm **b** Ag of 45 nm **c** Ag of 50 nm

Table 3 Measurement of R_{min} values for different Ag and Si thicknesses of structure-II

Ag Thickness	R_{min} values for respective Si thicknesses						
	1 nm	2 nm	3 nm	4 nm	5 nm	6 nm	7 nm
Ag = 40 nm	0.0305	0.0280	0.0245	0.0196	0.0117	0.0011	0.0559
Ag = 45 nm	0.0025	0.0032	0.0047	0.0076	0.0153	0.0465	0.3012
Ag = 50 nm	0.0699	0.0743	0.0809	0.0920	0.1157	0.1890	0.5550

Table 4 Different structures numbers and name and optimized thickness

Structure number and name	Thickness
I. Ag-Si-BP based	45 nm-6 nm-0.53 nm
II. Ag-Si-MXene based	40 nm-6 nm-0.993 nm

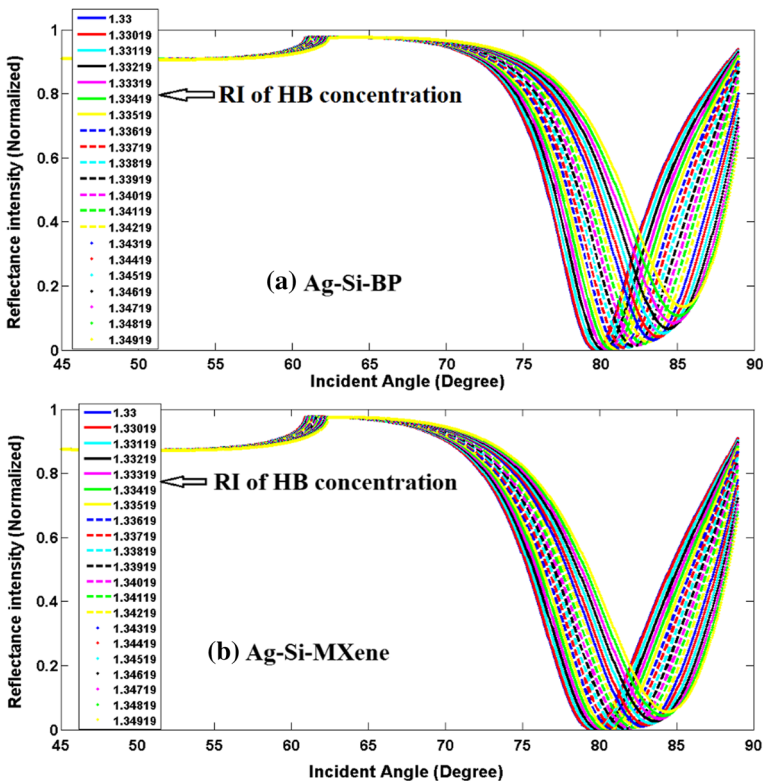


Fig. 8 Reflectance curves using angular interrogation for different RIs of blood HB concentrations **a** Ag-Si-BP **b** Ag-Si-MXene **c** Au-Si-BP **d** Au-Si-MXene

to the existed work. In HB in blood detection process, the heightened the performances are QF of 46.10 and DFOM of 3,511,000.00 for structure-I, and QF of 28.62 and DFOM of 3,858,333.33 for structure-II. Similarly, in glucose level in urine detection process, the

Table 5 Measured parameters of resonance angle and S for all structures (S-I, II, III, and IV significant for structures-I, II, III and IV) to detect the HB in blood

HB RI	θ_{res}		R_{min}		S ($^{\circ}/RIU$)		S ($^{\circ}/RIU$)		HB level (g/l)
	S-I	S-II	S-I	S-II	S-I	S-II	S-I	S-II	
1.33	79.67	79.49	0.00007	0.0011	–	–	–	–	Ref
1.33019	79.73	79.53	0.00009	0.0010	315.99	210.53	3,511,000.00	210,530.00	6.1025
1.33119	79.96	79.75	0.0003	0.0006	243.70	218.49	812,333.33	364,150.00	12.205
1.33219	80.20	79.97	0.0007	0.0003	242.00	219.18	345,714.29	730,600.00	18.3075
1.33319	80.50	80.19	0.0012	0.0001	260.19	219.44	216,825.00	2,194,400.00	24.410
1.33419	80.73	80.46	0.0020	0.0000	252.98	231.50	126,490.00	38,583,333.33	30.5125
1.33519	81.03	80.68	0.0030	0.0001	262.04	229.29	87,346.67	2,292,900.00	36.615
1.33619	81.26	80.94	0.0043	0.0003	258.54	234.25	60,125.58	780,833.33	42.7175
1.33719	81.56	81.20	0.0061	0.0007	262.87	237.83	43,093.44	339,757.14	48.820
1.33819	81.85	81.42	0.0083	0.0014	266.18	235.65	32,069.88	168,321.43	54.923
1.33919	82.15	81.69	0.0112	0.0025	269.86	239.39	24,094.64	95,756.00	61.025
1.34019	82.50	81.95	0.0148	0.0039	277.72	241.41	18,764.86	61,900.00	67.1275
1.34119	82.80	82.22	0.0193	0.0057	279.71	243.97	14,492.75	42,801.75	73.230
1.34219	83.09	82.53	0.0250	0.0082	280.56	249.39	11,222.40	30,413.41	79.333
1.34319	83.45	82.79	0.0321	0.0113	286.58	250.19	8927.73	22,140.70	85.435
1.34419	83.74	83.05	0.0411	0.0153	286.52	250.88	6971.29	16,397.39	91.538
1.34519	84.10	82.32	0.0525	0.0203	291.64	252.14	5555.05	12,420.69	97.640
1.34619	84.45	83.63	0.0665	0.0265	295.24	255.71	4439.70	9649.43	103.743
1.34719	84.81	83.89	0.0848	0.0342	299.00	255.96	3525.94	7484.21	109.845
1.34819	85.10	84.16	0.1075	0.0438	298.52	256.73	2776.93	5861.42	115.948
1.34919	85.40	84.46	0.1356	0.0556	298.59	258.99	2201.99	4658.09	122.050

heightened the performances are QF of 43.18 and DFOM of 57,500.00 for structure-I, and QF of 29.13 and DFOM of 135,000.00 for structure-II.

4.5 Electric field intensity performance analysis

Finally, this study evaluates the performance of the electric field intensity enhancement factor (EFIEF) for the proposed sensor. The EFIEF is a parameter that shows the origin of the S improvement, which was first investigated by A. Shalabney et al. in 2010 (Shalabney and Abdulhalim 2010).

$$EFIEF = \frac{\epsilon_1}{\epsilon_n} |t|^2 \tag{17}$$

The field intensity is inversely proportional to reflectivity, which implies that the field intensity’s maximum value is equal to the reflectivity’s minimum value. The maximal SPs excitation occurs near the location of strong EFIEF due to the lower R_{min} . The EFIEF performance is analyzed by applying Eq. (17) (Lin et al. 2020), and corresponding curves with respect to an angle are plotted in Fig. 12 for structure-I and II at the sensing RI of 1.33 and 1.335. The maximum achieved EFIEF performances for structure-I are 1.7192 and 1.6844 at the sensing RI of 1.33 and 1.335, respectively. Similarly, the EFIEF of 1.7158

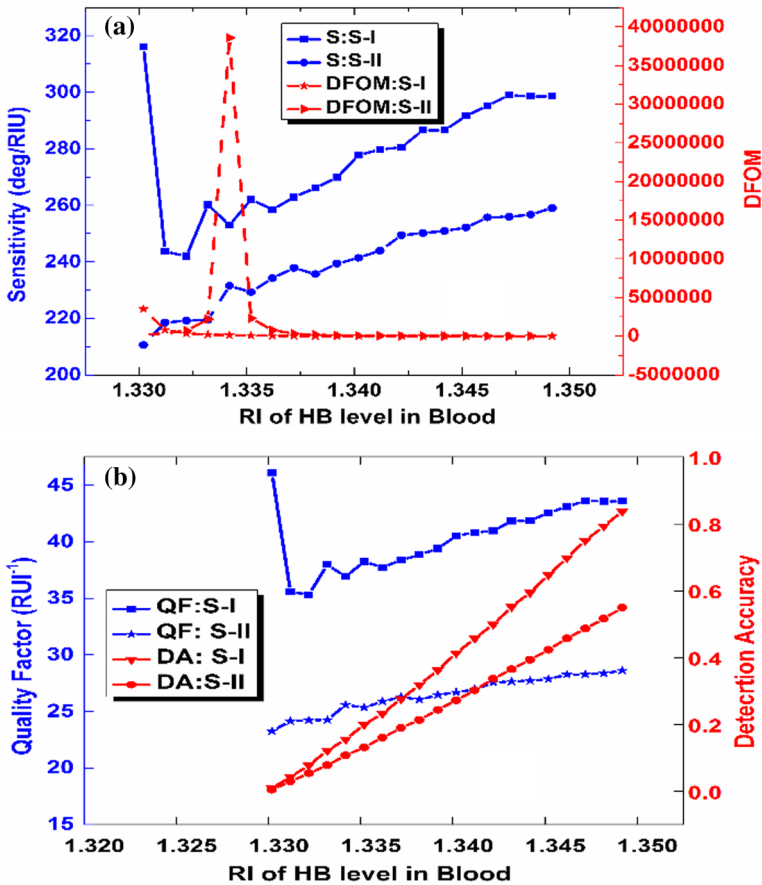


Fig. 9 Measured parameters for structure-I and II with respect to the RI of HB level in urine: **a** S and DFOM **b** QF and DA

and 1.6937 for structure-II at the sensing RI of 1.33 and 1.335, respectively. From this study, it can be confirmed the proposed work facilitates a better EFIEF performance at lower sensing RI, and the EFIEF performance is inversely proportional to the sensing RI. Therefore, the proposed SPR sensor can be utilized in biomedical applications like biological samples detection in order to sense the very small deviation in the SPR structure as well as to accomplish a better SPR performance.

5 Conclusions

The numerical modeling of SCHOTT B270 prism-based “surface plasmon resonance (SPR)” sensor is presented using “silver (Ag)-silicon (Si)-black phosphorus (BP)/ carbides and nitrides (MXene)” structure to detect the hemoglobin (HB) in blood and urine glucose level in this paper. This study has been carried out with two different structures, such as structure-I and II, which are made with defined materials. The performances of boron 270 (B270) and boron kron-7 (BK7) prism-based structures have been analyzed

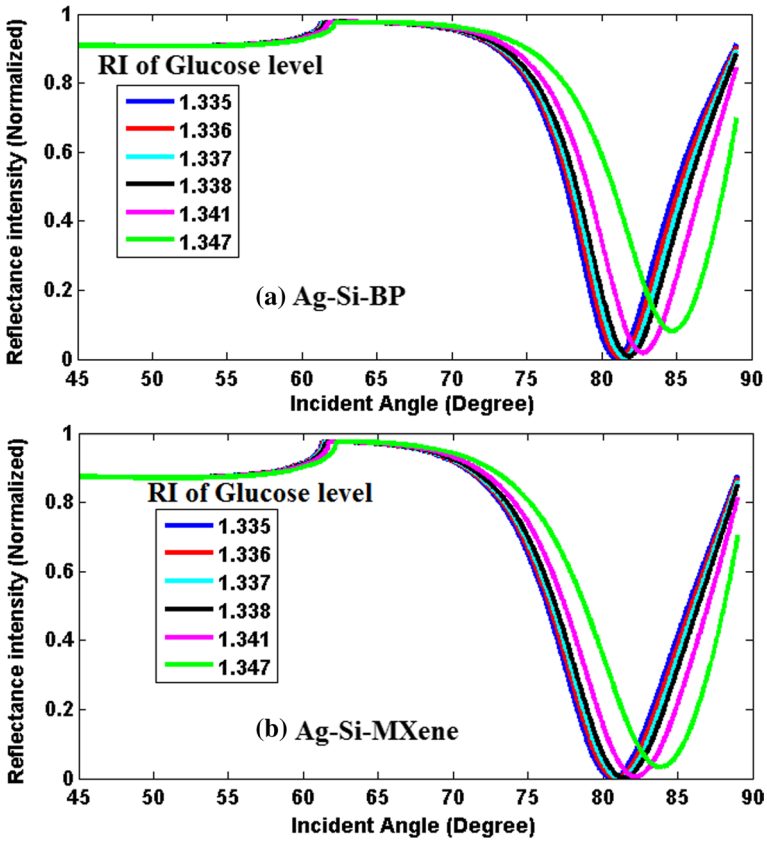


Fig. 10 Reflectance curves using angular interrogation for different RIs of glucose level in urine a Ag-Si-BP b Ag-Si-MXene c Au-Si-BP d Au-Si-MXene

Table 6 Measured parameters of resonance angle and s for all structures (S-I, II, III, and IV significant for structures-I, II, III and IV) to detect the glucose level in urine

Glucose level RI	θ_{res}		R_{min}		$S (^{\circ}/RIU)$		DFOM		Glucose level (mg/dl)
	S-I	S-II	S-I	S-II	S-I	S-II	S-I	S-II	
1.335	80.97	80.63	0.0025	0.00004	-	-	-	-	Ref
1.336	81.20	80.90	0.0040	0.0002	230	270	57,500.00	1,350,000.00	0.625
1.337	81.50	81.16	0.0057	0.0006	265	265	46,491.12	441,666.67	1.25
1.338	81.79	81.38	0.0078	0.0013	273.33	250	35,042.30	192,307.69	2.5
1.341	82.74	82.17	0.0184	0.0053	295	256.67	16,032.61	48,428.30	5
1.347	84.69	83.85	0.0811	0.0326	310	268.33	3822.44	8230.98	10

by plotting reflectance curves using the angular interrogation technique. It is noticed the optimal performances in terms of “sensitivity (S)” and “minimum reflectance (R_{min})” are accomplished for B270 prism-based structure. Furthermore, the performances of

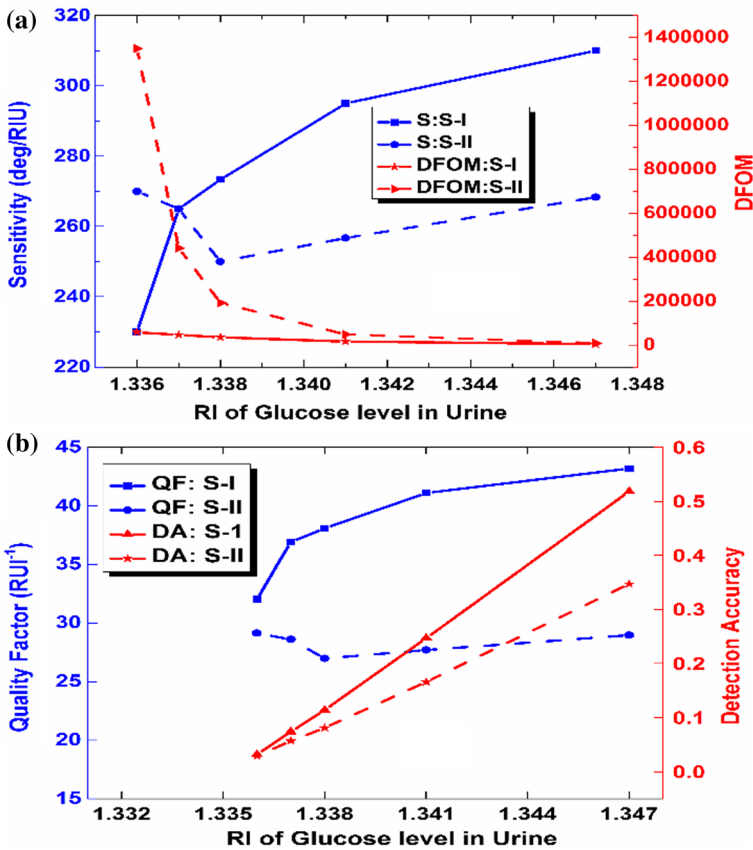


Fig. 11 Measured parameters for structure-I and II with respect to the RI of glucose level in urine: **a** S and DFOM **b** QF and DA

detection processes of specific biological samples have been analyzed in terms of S, “detection accuracy (DA)”, “quality factor (QF)” and “dip-of-figure of merit (DFOM)”. The HB in blood detection shows the maximum S of 315.79 and 258.99 deg/RIU, DA of 0.837 and 0.549, QF of 46.10 and 28.62 RIU⁻¹, and DFOM of 3,511,000.00 and 38,583,333.33 for structure-I and II, respectively. Similarly, the urine glucose detection furnishes the maximum S of 310 and 270 deg/RIU, DA of 0.518 and 0.347, QF of 43.18 and 29.13 RIU⁻¹, and DFOM of 57,500.00 and 1,350,000.00 for structure-I and II, respectively. Finally, the comparative study has been carried out, which demonstrates the proposed work that heightened the performances of S and DA, and presents the QA and DFOM performances for the first time compared to the existed work. Therefore, the proposed SPR sensor can be used as a high-performance candidate to the biological samples detection and establishes a new platform in the biomedical and biological fields.

Table 7 The performance of proposed work and existed work comparison on the detection of HB in blood and glucose in urine at 633 nm

Reference	Structure	Detection of HB level in blood				Detection of glucose level in urine			
		S (deg/RIU)	DA	QF (RIU ⁻¹)	DFOM	S (deg/RIU)	DA	QF (RIU ⁻¹)	DFOM
S. Mustufa et al. (Shahriar et al. 2021)	BK7-Au-PtSe2-Graphene-Sensing	200.00	0.094	-	-	166.67	0.093	-	-
Proposed Work	B270-Ag-Si-BP-Sensing	315.79	0.837	46.10	3,511,000.00	310.00	0.518	43.18	57,500.00
Proposed Work	B270-Ag-Si-MIXene-Sensing	258.99	0.549	28.62	38,583,333.33	270.00	0.347	29.13	1,350,000.00

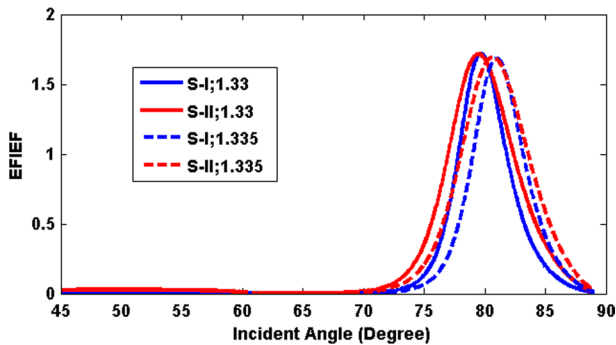


Fig.12 EFIEF versus angle for all defined-structures at sensing RI of 1.33 and 1.335

Acknowledgements This research did not receive any specific grant from funding agencies in the public, commercial, or not-for-profit sectors.

Funding The authors have not disclosed any funding.

Declarations

Conflict of interest The authors have not disclosed any competing interests.

References

- Ahmed, K., Ahmed, F., Roy, S., Paul, B.K., Aktar, M.N., Vigneswaran, D., Islam, M.S.: Refractive index-based blood components sensing in terahertz spectrum. *J. IEEE Sensors* **19**(9), 3368–3375 (2019c). <https://doi.org/10.1109/JSEN.2019.2895166>
- Ahmed, K., Paul, B.K., Vasudevan, B., Rashed, A.N., Maheswar, R., Amiri, I.S., Yupapin, P.: Design of D-shaped elliptical core photonic crystal fiber for blood plasma cell sensing application. *Results in Phys.* **12**, 2021–2025 (2019a). <https://doi.org/10.1016/j.rinp.2019.02.026>
- Ahmed, K., Haque, M.J., Jabin, M.A., Paul, B.K., Amiri, I.S., Yupapin, P.: Tetra-core surface plasmon resonance based biosensor for alcohol sensing. *Physica B* **570**, 48–52 (2019b). <https://doi.org/10.1016/j.physb.2019.05.047>
- Ahmed, K., AlZain, M.A., Abdullah, H., Luo, Y., Vigneswaran, D., Faragallah, O.S., Eid, M.M., Rashed, A.N.: Highly sensitive twin resonance coupling refractive index sensor based on gold-and MgF₂-coated nano metal films. *Biosensors* **11**(4), 104 (2021). <https://doi.org/10.3390/bios11040104>
- Ajad, A.K., Islam, M.J., Kaysir, M.R., Atai, J.: Highly sensitive bio sensor based on WGM ring resonator for hemoglobin detection in blood samples. *Optik* **226**, 166009 (2021). <https://doi.org/10.1016/j.ijleo.2020.166009>
- Biednov, M., Lebedeva, T., Shpilovuy, P.: Gold and Aluminum based surface Plasmon resonance biosensors: sensitivity enhancement. *Opt. Sens.* **9506**, 95061P (2015). <https://doi.org/10.1117/12.2177992>
- Cai, H., Shan, S., Wang, X.: High sensitivity surface plasmon resonance sensor based on periodic multilayer thin films. *Nanomater.* **11**(12), 3399 (2021). <https://doi.org/10.3390/nano11123399>
- Cho, S.Y., Lee, Y., Koh, H.J., Jung, H., Kim, J.S., Yoo, H.W., Kim, J., Jung, H.J.: Superior chemical sensing performance of black phosphorus: comparison with MoS₂ and graphene. *Adv. Mater.* **28**(32), 7020–7028 (2016). <https://doi.org/10.1002/adma.201601167>
- Farimani, A.B., Min, K., Aluru, N.R.: DNA base detection using a single-layer MoS₂. *ACS Nano* **8**, 7914–7922 (2014). <https://doi.org/10.1021/nn5029295>
- Homola, J.: Surface plasmon resonance biosensors for food safet. *Opt. Sens. Chem. Sens. Biosens.* (2004). <https://doi.org/10.1016/j.bios.2019.111449>
- Homola, J.: Surface plasmon resonance based sensors. *Chem. Sens. Biosen.* **4**, 45–67 (2006). <https://doi.org/10.1007/5346-014>

- Hossain, M.B., Akib, T.B., Abdulrazak, L.F., Rana, M.M.: Numerical modeling of graphene-coated fiber optic surface plasmon resonance biosensor for BRCA1 and BRCA2 genetic breast cancer detection. *Opt. Eng.* **58**(3), 037104 (2019a). <https://doi.org/10.1117/1.OE.58.3.037104>
- Hossain, M.B., Islam, M.M., Abdulrazak, L.F., Rana, M.M., Akib, T.B.A., Hassan, M.: "Graphene coated optical fiber SPR biosensor for BRCA1 and BRCA2 breast cancer biomarker detection: a numerical design-based analysis. *Phot. Sens.* **10**(2), 1–13 (2019b). <https://doi.org/10.1007/s13320-019-0556-7>
- Jabbari, S., Dabirmanesh, B., Arab, S.S., Amanlou, M., Daneshjou, S., Gholami, S., Khajeh, K.: A novel enzyme based SPR biosensor to detect bromocriptine as an ergoline derivative drug. *Sens. Act. B Chem.* **240**, 519–527 (2016). <https://doi.org/10.3390/bios11020043>
- Jabin, M., Ahmed, K., Rana, M., Paul, B.K., Luo, Y., Vigneswaran, D.: Titanium-coated dual-core D-shaped SPR-based PCF for hemoglobin sensing. *Plasmonics* **14**(6), 1601–1610 (2019a). <https://doi.org/10.1007/s11468-019-00961-6>
- Jabin, M.A., Ahmed, K., Rana, M.J., Paul, B.K., Islam, M., Vigneswaran, D., Uddin, M.S.: Surface plasmon resonance based titanium coated biosensor for cancer cell detection. *J IEEE Phot. Jun* **11**(4), 1–10 (2019b). <https://doi.org/10.1109/JPHOT.2019.2924825>
- Jabin, M., Rana, M., Al-Zahrani, F.A., Paul, B.K., Ahmed, K., Bui, F.M.: Novel detection of diesel adulteration using silver-coated surface plasmon resonance sensor. *Plasmonics* **17**(2), 467–478 (2022). <https://doi.org/10.1007/s11468-021-01540-4>
- Jouven, X., Lemaître, R.N., Rea, T.D., Sotoodehnia, N., Empana, J.P., Siscovick, D.S.: Diabetes, 297 glucose level, and risk of sudden cardiac death. *Eur. Heart J.* **26**, 2142–2147 (2005). <https://doi.org/10.1093/eurheartj/ehi376>
- Klantsataya, E., François, A., Ebendorff-Heidepriem, H., Hoffmann, P., Monro, T.M.: Surface plasmon scattering in exposed core optical fiber for enhanced resolution refractive index sensing. *Sensors* **15**(10), 25090–25102 (2015). <https://doi.org/10.3390/s151025090>
- Kretschmann, E., Raether, H.: Notizen: radiative decay of non radiative surface plasmons excited by light. *Spr. Z Natur.* **23**(A), 2135–2136 (1968). <https://doi.org/10.1515/zna-1968-1247>
- Kumar, R., Pal, S., Pal, N., Mishra, V., Prajapati, Y.K.: High-performance bimetallic surface plasmon resonance biochemical sensor using a black phosphorus–MXene hybrid structure. *Appl. Phys. a* **127**, 1–2 (2021). <https://doi.org/10.1007/s00339-021-04408-w>
- Kumar, R., Pal, S., Prajapati, Y.K., Kumar, S., Saini, J.P.: Sensitivity improvement of a MXene-immobilized SPR sensor with Ga-doped-ZnO for biomolecules detection. *J. IEEE Sensors* **22**(7), 6536–6543 (2022). <https://doi.org/10.1109/JSEN.2022.3154099>
- Lee, K.L., Wu, S.H., Lee, C.W., Wei, P.K.: Sensitive biosensors using Fano resonance in single gold nanoslit with periodic grooves. *Opt. Exp.* **19**(24), 24530–24539 (2011). <https://doi.org/10.1364/OE.19.024530>
- Liang, M., Zhang, M., Yu, S., Wu, Q., Ma, K., Chen, Y., Liu, X., Li, C., Wang, F.: Silver-laden black phosphorus nanosheets for an efficient in vivo antimicrobial application. *Small* **16**(13), 1905938 (2020). <https://doi.org/10.1002/smll.201905938>
- Lin, Z., Chen, S., Lin, C.: Sensitivity improvement of a surface plasmon resonance sensor based on two-dimensional materials hybrid structure in visible region: a theoretical study. *Sensors* **20**(9), 2445 (2020). <https://doi.org/10.3390/s20092445>
- Mao, N., Tang, J., Xie, L., Wu, J., Han, B., Lin, J., Deng, S., Ji, W., Xu, H., Liu, K., Tong, L.: Optical anisotropy of black phosphorus in the visible regime. *Ame. Chem. Soc.* **138**(1), 300–305 (2016). <https://doi.org/10.1021/jacs.5b10685>
- Masson, J.F.: Surface Plasmon resonance clinical biosensors for medical diagnostics. *ACS Sens.* **2**(1), 16–30 (2017). <https://doi.org/10.1021/acssensors.0c02729j>
- Maurya, J.B., Prajapati, Y.K.: Influence of dielectric coating on performance of surface plasmon resonance sensor. *Plasmonics* **12**(4), 1121–1130 (2017 Aug). <https://doi.org/10.1007/s11468-016-0366-3>
- Maurya, J.B., Prajapati, Y.K.: Experimental demonstration of DNA hybridization using graphene based plasmonic sensor chip. *J. Lightwave Technol.* **38**(18), 5191–5198 (2020). <https://doi.org/10.1109/JLT.2020.2998138>
- Mishra, A.K., Mishra, S.K., Verma, R.K.: Graphene and beyond graphene MoS₂: a new window in surface-plasmon-resonance-based fiber optic sensing. *J. Phys. Chem. C* **120**(5), 2893–2900 (2016). <https://doi.org/10.1021/acs.jpcc.5b08955>
- Mitu, S.A., Aktar, M., Ibrahim SM, S.M., Ahmed, K.: Surface plasmon resonance-based refractive index biosensor: an external sensing approach. *Plasmonics* (2022). <https://doi.org/10.1007/s11468-022-01645-4>

- Mitu, S.A., Ahmed, K., Al Zahrani, F.A., Grover, A., Rajan, M.S., Moni, M.A.: Development and analysis of surface plasmon resonance based refractive index sensor for pregnancy testing. *Opt. Las. Eng.* **140**, 106551 (2021). <https://doi.org/10.1016/j.optlaseng.2021.106551>
- Mudgal, N., Yupapin, P., Ali, J., Singh, G.: BaTiO₃-Graphene-Affinity Layer-Based Surface Plasmon Resonance (SPR) Biosensor for Pseudomonas Bacterial Detection. *Plasmonics* **2**, 1–9 (2020). <https://doi.org/10.1007/s11468-020-01146-2>
- Otto, A.: Excitation of surface plasma waves in silver by the method of frustrated total reflection. *Spr. Z Phys.* **216**, 398–410 (1968). <https://doi.org/10.1007/BF01391532>
- Paul, B.K., Rajesh, E., Asaduzzaman, S., Islam, M.S., Ahmed, K., Amiri, I.S., Zakaria, R.: Design and analysis of slotted core photonic crystal fiber for gas sensing application. *Results in Phys.* **11**, 643–650 (2018). <https://doi.org/10.1016/j.rinp.2018.10.004>
- Perez, M.A., Gonzalez, O., Arias, J.R.: Optical fiber sensors for chemical and biological measurements. *Curr. Dev. Opt. Fiber. Technol.* (2013). <https://doi.org/10.5772/52741>
- Rahman, M.S., Anower, M.S., Rahman, M.K., Hasan, M.R., Hossain, M.B., Haque, M.I.: Modeling of highly sensitive MoS₂-graphene hybrid based fiber optic SPR biosensor for sensing DNA hybridization. *Optik* **140**, 989–997 (2017a). <https://doi.org/10.1016/j.jjleo.2017.05.001>
- Rahman, M.S., Anower, M.S., Hasan, M.R., Hossain, M.B., Haque, M.I.: Design and numerical analysis of highly sensitive Au-MoS₂ graphene based hybrid surface plasmon resonance biosensor. *Opt. Comm.* **396**, 36–43 (2017b). <https://doi.org/10.1016/j.optcom.2017.03.035>
- Rahman, M.S., Anower, M.S., Abdulrazak, L.F., Rahman, M.M.: Modeling of a fiber-optic surface plasmon resonance biosensor employing phosphorene for sensing applications. *Opt. Eng.* **58**(3), 037103 (2019). <https://doi.org/10.1117/1.OE.58.3.037103>
- Said, F.A., Menon, P.S., Kalaivani, T., Mohamed, M.A., Abedini, A., Shaari, S., Majlis, B.Y., Retnasamy, V.: FDTD analysis of structured metallic nanohole films for LSPR-based biosensor. *IEEE RSM* (2015). <https://doi.org/10.1109/RSM.2015.7355024>
- Sani, M.H., Khosroabadi, S.: A novel design and analysis of high-sensitivity biosensor based on nanocavity for detection of blood component, diabetes, cancer and glucose concentration. *IEEE Sens. J.* **20**, 7161–7168 (2020a). <https://doi.org/10.1109/JSEN.2020.2964114>
- Sani, M.H., Khosroabadi, S.: A novel design and analysis of high-sensitivity biosensor based on 300 nano-cavity for detection of blood component, diabetes, cancer and glucose concentration. *IEEE 301 Sens J* **20**, 7161–7168 (2020b). <https://doi.org/10.1109/JSEN.2020.2964114>
- Shahriar, M., Paul, A.K., Chakrabarti, K.: Detection of hemoglobin in blood and urine glucose level samples using a graphene-coated SPR based biosensor. *OSA Contin.* **4**, 2164–2176 (2021). <https://doi.org/10.1364/OSAC.433633>
- Shalabney, A., Abdulhalim, I.: Electromagnetic fields distribution in multilayer thin film structures and the origin of sensitivity enhancement in surface plasmon resonance sensors. *Sens. Act. A Phys.* **159**, 24–32 (2010). <https://doi.org/10.1016/j.sna.2010.02.005>
- Sharma, A.K., Pandey, A.K.: Blue phosphorene/MoS₂ heterostructure based SPR sensor with enhanced sensitivity. *IEEE Phot. Techn. Lett.* **30**(7), 595–598 (2018). <https://doi.org/10.1109/LPT.2018.2803747>
- Singh, M.K., Pal, S., Verma, A., Mishra, V., Prajapati, Y.K.: Sensitivity enhancement using anisotropic black phosphorus and antimonene in bi-metal layer-based surface plasmon resonance biosensor. *Superl. Microstruct.* **156**, 106969 (2021). <https://doi.org/10.1016/j.spmi.2021.106969>
- Srivastava, A., Verma, A., Das, R., Prajapati, Y.K.: A theoretical approach to improve the performance of SPR biosensor using MXene and black phosphorus. *Optik* **203**, 163430 (2020). <https://doi.org/10.1016/j.jjleo.2019.163430>
- Vasimalla, Y., Pradhan, H.S., Pandya, R.J.: Recent progress in surface plasmon resonance based sensors: A comprehensive review. *Heliyon*. **7**, e06321 (2021a). <https://doi.org/10.1016/j.heliyon.2021.e06321>
- Vasimalla, Y., Pradhan, H.S., Pandya, R.J.: Sensitivity enhancement of the SPR biosensor for Pseudomonas bacterial detection employing a silicon-barium titanate structure. *Appl. Opt.* **60**, 5588–5598 (2021b). <https://doi.org/10.1364/AO.427499>
- Vasimalla, Y., Pradhan, H.S., Pandya, R.J.: SPR performance enhancement for DNA hybridization employing black phosphorus, silver and silicon. *Appl. Opt.* **59**, 7299–7307 (2020). <https://doi.org/10.1364/AO.397452>
- Wu, L., Guo, J., Wang, Q., Lu, S., Dai, X., Xiang, Y., Fan, D.: Sensitivity enhancement by using few-layer black phosphorus-graphene/ TMDCs heterostructure in surface plasmon resonance biochemical sensor. *Sen. Actua. B Chem.* **249**, 542–548 (2017). <https://doi.org/10.1016/j.snb.2017.04.110>
- Xin, M., Li, J., Ma, Z., Pan, L., Shi, Y.: MXenes and their applications in wearable sensors. *Frontiers in Chem.* **21**, 297 (2020). <https://doi.org/10.3389/fchem.2020.00297>

- Yola, M.I., Atar, N., Eren, T.: Determination of amikacin in human plasma by molecular imprinted SPR nanosensor. *Sens. Actuators B Chem.* **198**, 70–76 (2014). <https://doi.org/10.1016/j.snb.2014.02.107>
- Zakaria, R., Zainuddin, N.A., Ahmad Fahri, M.A., Kamkar, A., Al Zahrani, F.A., Patel, S.K., Ahmed, K.: Exploration of multi-metallic thin layer/MgF₂ in side-polished optical fiber as long-range surface plasmons (LRSPs) alcohol sensor. *Opt. Quant. Electron.* **54**(4), 1–6 (2022). <https://doi.org/10.1007/s11082-022-03614-x>

Publisher's Note Springer Nature remains neutral with regard to jurisdictional claims in published maps and institutional affiliations.

Springer Nature or its licensor holds exclusive rights to this article under a publishing agreement with the author(s) or other rightsholder(s); author self-archiving of the accepted manuscript version of this article is solely governed by the terms of such publishing agreement and applicable law.

Authors and Affiliations

Yesudasu Vasimalla¹  · Himansu Shekhar Pradhan²

Himansu Shekhar Pradhan
hsp@nitw.ac.in

- ¹ Koneru Lakshmaiah Educational Foundation (KLEF), Vaddeswaram, Andhra Pradesh 522302, India
- ² National Institute of Technology, Warangal, Telangana 506004, India